Quantum Optimization via Four-Body Rydberg Gates

Clemens Dlaska, Kilian Ender, Glen Bigan Mbeng, Andreas Kruckenhauser, Wolfgang Lechner, and Rick van Bijnen

Phys. Rev. Lett. **128**, 120503 — Published 24 March 2022

DOI: 10.1103/PhysRevLett.128.120503

Quantum optimization via four-body Rydberg gates

Clemens Dlaska,[1,2] Kilian Ender,[1,3] Glen Bigan Mbeng,[1]
Andreas Kruckenhauser,[2,4] Wolfgang Lechner,[1,3] and Rick van Bijnen[2,4]

[1] *Institute for Theoretical Physics, University of Innsbruck, A-6020 Innsbruck, Austria*
[2] *Institute for Quantum Optics and Quantum Information of the Austrian Academy of Sciences, A-6020 Innsbruck, Austria*
[3] *Parity Quantum Computing GmbH, A-6020 Innsbruck, Austria*
[4] *Center for Quantum Physics, Faculty of Mathematics, Computer Science and Physics, University of Innsbruck, 6020 Innsbruck, Austria*

A large ongoing research effort focuses on obtaining a quantum advantage in the solution of combinatorial optimization problems on near-term quantum devices. A particularly promising platform implementing quantum optimization algorithms are arrays of trapped neutral atoms, laser-coupled to highly excited Rydberg states. However, encoding combinatorial optimization problems in atomic arrays is challenging due to limited inter-qubit connectivity of the native finite-range interactions. Here we present a four-body Rydberg parity gate, enabling a direct and straightforward implementation of the parity architecture, a scalable architecture for encoding arbitrarily connected interaction graphs. Our gate relies on adiabatic laser pulses and is fully programmable by adjusting two hold-times during operation. We numerically demonstrate implementations of the quantum approximate optimization algorithm (QAOA) for small-scale test problems. Variational optimization steps can be implemented with a constant number of system manipulations, paving the way for experimental investigations of QAOA beyond the reach of numerical simulations.

Introduction– Currently available quantum devices are capable of generating controlled dynamics challenging numerical simulations on even the most powerful classical supercomputers [1–3]. These quantum devices will have up to a few hundred qubits available, without error correction, and have been termed Noisy Intermediate Scale Quantum (NISQ) devices. A key challenge for the field of quantum technology at this very moment is to find ways of putting the computational power of near-term quantum devices to good use [4, 5]. In this era of NISQ devices, the development of specialized algorithms, targeting specific problems that provide a structural match with the strengths of a particular quantum platform, is thus highly desirable. A strategy of co-design of algorithms and experimental platforms aims at developing scientifically and industrially relevant applications in the near term, before the need for error correction arises.

Here we focus on designing specialized quantum hardware for solving combinatorial optimization problems, using neutral atoms trapped in tweezer arrays, laser-coupled to highly excited Rydberg states [6–15]. The Rydberg states provide strong and tunable interactions, that can be switched on and off by coherently coupling ground and Rydberg states. Combined with single particle operations, the interactions form appealing building blocks for QAOA [16, 17]. There, the goal is to find approximate solutions to combinatorial optimization problems, cast in the form of energy minimization of a general N-spin problem Hamiltonian

$$\hat{H}_P = \sum_i J_i \hat{\sigma}_z^{(i)} + \sum_{i<j} J_{ij} \hat{\sigma}_z^{(i)} \hat{\sigma}_z^{(j)} + \sum_{i<j<k} J_{ijk} \hat{\sigma}_z^{(i)} \hat{\sigma}_z^{(j)} \hat{\sigma}_z^{(k)} + \dots, \tag{1}$$

where $\hat{\sigma}_{\{x,y,z\}}$ denote the Pauli spin operators and $\{J_i, J_{ij}, J_{ijk}, \dots\}$ are local fields and long-ranged higher-order interactions. QAOA attempts to find low energy solutions, by driving a system of quantum spins alternately with a driver Hamiltonian $\hat{H}_X = \sum_i \hat{\sigma}_x^{(i)}$ and the problem Hamiltonian $\hat{H}_P$.

Despite the recent universality and quantum advantage results [18–20], various aspects of QAOA's performance are still under theoretical investigation [21]. On the one hand the existence of barren plateaus [22] and reachability deficits [23–25] suggest strong limitations for QAOA while, on the other hand, parameter concentration effects [26–30] may boost the algorithm's efficiency. Ultimately, due to QAOA's heuristic nature, its practical performance in a regime beyond the capability of classical computers is difficult to predict and requires to be experimentally tested.

Recent advances in Rydberg experiments, such as coherent control of atomic states and deterministic atom positioning of hundreds of atoms, make the Rydberg platform a particularly promising target for such investigations. Direct experimental implementations of QAOA with Rydberg atoms are, however, limited by the binary nature of the Rydberg interaction and their polynomially decaying interaction strengths, which only admit scalable experimental implementations of $\hat{H}_P$ for very specific problems [8, 31].

Instead of attempting to directly engineer the spin model version of $\hat{H}_P$, we adopt the parity architecture [32, 33], a scalable and problem independent quantum hardware blueprint for generic combinatorial optimization problems. Running QAOA then only requires problem dependent single-qubit gates and problem independent multi-qubit phase-gates acting on three or four qubits at the corners of 2×2 plaquettes as (cf. Fig. 1) $U_{\boxtimes}(\gamma) = e^{i\gamma \prod_k \hat{\sigma}_z^{(k)}}$, where the latter do not naturally

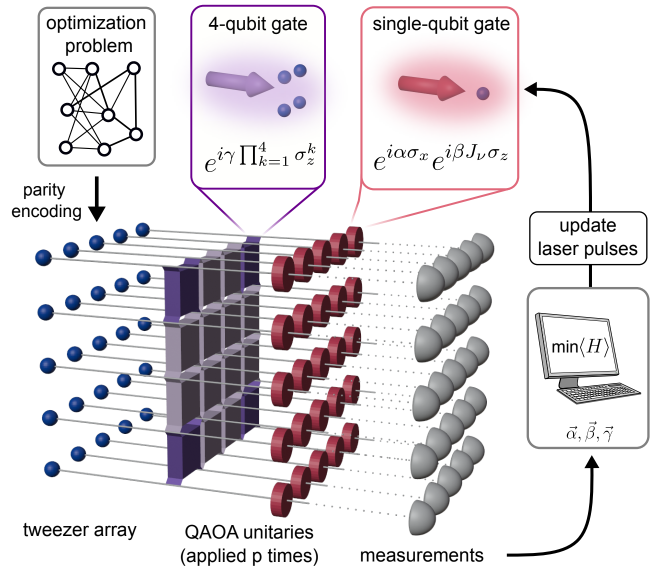

FIG. 1. *Rydberg parity QAOA protocol.* Arbitrarily connected optimization problems can be parity encoded in a regular geometry of neutral atoms trapped in e.g. optical tweezers. After initializing the Rydberg quantum processor in an equal superposition state, generating variational wave functions by applying QAOA unitaries only requires local control of laser fields generating quasi-local four- (square boxes) and single-qubit gates (discs).

exist on the Rydberg platform.

In the following we show how such a gate can be directly engineered between ground state atoms utilizing time-optimal adiabatic laser-coupling to Rydberg states, i.e. without relying on (distinct species) auxiliary qubits [34] or decomposition into two-body gates [35]. We provide a simple two-pause strategy to program arbitrary phases γ subsequent to a onetime optimization of laser-ramps within parameter-limits given by particular experiments. The entire QAOA can then be implemented on present-day experiments as an optimization of the duration of laser pulses. Below we explain the details and performance of our scheme, and give a numerical demonstration of the QAOA protocol on the Rydberg platform.

Rydberg parity QAOA– The parity hardware architecture provides a blueprint for a problem independent and scalable quantum processor that is tailored to tackle generic combinatorial optimization problems (see Supplemental Material (SM) [36] for a detailed introduction). In short, parity-qubits encode the relative orientation, i.e. the parity, of spins representing the optimization problem, with $J_{ij}\hat{\sigma}_z^{(i)}\hat{\sigma}_z^{(j)} \rightarrow J_\mu\hat{\sigma}_z^{(\mu)}$, $J_{ijk}\hat{\sigma}_z^{(i)}\hat{\sigma}_z^{(j)}\hat{\sigma}_z^{(k)} \rightarrow J_\nu\hat{\sigma}_z^{(\nu)}$ etc., replacing long-range interactions $\{J_{ij}, J_{ijk}, \dots\}$ by local-fields $\{J_\mu, J_\nu, \dots\}$. Since the parity transformation increases the number of qubits to the number K of interactions present in the optimization problem, the original N-qubit code-space needs to be stabilized by quasi-local three- or four-qubit stabilizers of the form $H_{\boxplus} \propto \prod_{\mu=1}^{l}\hat{\sigma}_z^{(\mu)}$ (i.e. $l = 3, 4$), that act as energetic constraints on 2×2 plaquettes [33, 37].

Implementations of QAOA for parity encoded optimization problems rely on alternately driving the quantum spin system, prepared in the $|+\rangle^{\otimes K}$ state, with a driving Hamiltonian and the problem Hamiltonian. While the single qubit driving Hamiltonian $\hat{H}_X = \sum_\nu^K \hat{\sigma}_x^{(\nu)}$ remains as before, the problem Hamiltonian $\hat{H}_P$ is now decomposed into a single qubit problem encoding $\hat{H}_Z = \sum_\nu^K J_\nu\hat{\sigma}_z^{(\nu)}$, and a quasi local constraint term $\hat{H}_C = \sum_{\boxplus} H_{\boxplus}$, where the sum runs over all 2×2 plaquettes denoted by $\boxplus$. Alternately applying each of the Hamiltonian operators p times, QAOA thus generates states

$$|\psi(\boldsymbol{\alpha},\boldsymbol{\beta},\boldsymbol{\gamma})\rangle = \prod_{j=1}^{p} e^{-i\alpha_j\hat{H}_X} e^{-i\beta_j\hat{H}_Z} e^{-i\gamma_j\hat{H}_C} |+\rangle^{\otimes K}, \quad (2)$$

where variational parameters α_j, β_j, and γ_j ($j = 1, 2, \dots, p$) determine the duration of driving with $\hat{H}_X, \hat{H}_Z, \hat{H}_C$, respectively. Low-energy solutions to the original optimization problem are then determined in a quantum-classical feedback loop, where a classical computer optimizes the parameters $(\boldsymbol{\alpha},\boldsymbol{\beta},\boldsymbol{\gamma})$, based on energy estimation obtained by repeated single qubit measurements in the z-direction.

The quantum spin system we have in mind consists of a regular array of trapped neutral atoms, e.g. Rubidium (^{87}Rb) atoms trapped in optical tweezers (cf. Fig. 1). Each atom realizes a qubit by encoding the qubit basis $\{|\downarrow\rangle, |\uparrow\rangle\}$ in a pair of atomic ground states (e.g. two hyperfine states). We assume the ability to locally address atoms with targeted laser light, e.g. by using spatial light modulators (SLMs) [13, 38–40]. The single particle operations $\hat{H}_Z$ can then be implemented through AC Stark shifts from laser coupling to low-lying excited states. The driver Hamiltonian $\hat{H}_X$ can be implemented through Raman transitions. In the following, we discuss the Rydberg implementation of the key nontrivial component, the many-body phase gate $e^{-i\gamma\hat{H}_C}$.

Four-qubit parity gate implementation– The main challenge for experimental realizations of the parity-QAOA algorithm is a direct and straightforward implementation of the four-qubit gate $U_{\boxplus}(\gamma) = e^{-i\gamma H_{\boxplus}}$. The operator $H_{\boxplus}$ energetically separates plaquette states $|z_{\text{even}}\rangle$ with an even number of particles in the $|\downarrow\rangle$ state, from plaquette states $|z_{\text{odd}}\rangle$ with an odd number of particles in the state $|\downarrow\rangle$. The desired gate operation $U_{\boxplus}(\gamma)$ thus corresponds to a four-qubit phase gate, mapping the plaquette states as follows:

$$\begin{aligned} U_{\boxplus}(\gamma)\,|z_{\text{odd}}\rangle &= e^{i\gamma}\,|z_{\text{odd}}\rangle\,, \\ U_{\boxplus}(\gamma)\,|z_{\text{even}}\rangle &= e^{-i\gamma}\,|z_{\text{even}}\rangle\,. \end{aligned} \quad (3)$$

We propose to implement $U_{\boxplus}(\gamma)$ with an adiabatic protocol, such that each computational state acquires a controllable dynamical phase $|z\rangle \rightarrow e^{i\Phi_z}|z\rangle$, designed to match Eq. (3) for arbitrary angles γ.

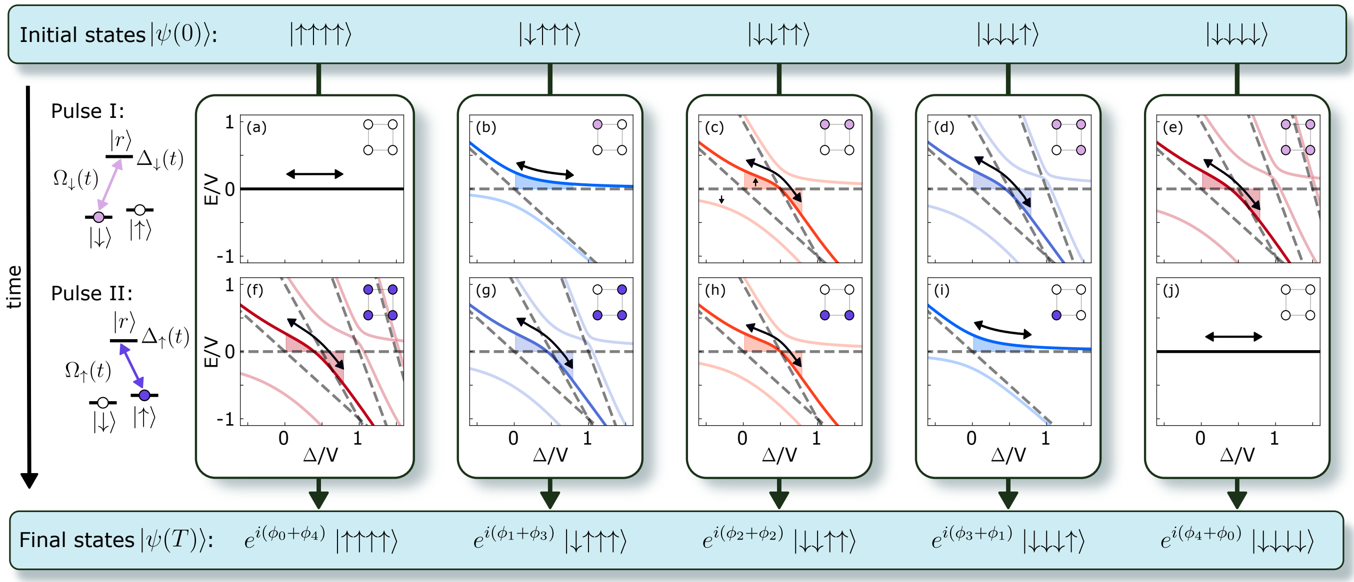

FIG. 2. Four-body Rydberg gate protocol. The laser-parameter dependent plaquette energy-spectrum exhibits distinct behavior w.r.t. the number of laser-excitable spins (indicated by , , . . .). Solid (dashed) lines show the energy-spectrum as function of the laser detuning $\Delta_{\downarrow,\uparrow}$ for a fixed Rabi-frequency of $\Omega_{\downarrow,\uparrow} = V/2$ ($\Omega_{\downarrow,\uparrow} = 0$). Applying an adiabatic, time dependent laser pulse $(\Omega_\downarrow(t), \Delta_\downarrow(t))$ addressing qubit state $|\downarrow\rangle$ imprints an excitation-sector dependent dynamical phase ϕ_n on the corresponding computational basis states (upper row). For constant Rydberg interaction strengths between plaquette atoms, subsequently applying the same adiabatic laser pulse on qubit states $|\uparrow\rangle$ leads to the desired phase separation of even and odd parity configurations (bottom line).

We will show that this operation can be implemented with two adiabatic laser pulses, with time-dependent intensity and detuning, where a first pulse couples only the $|\downarrow\rangle$ states to a Rydberg level $|r\rangle$, and the second pulse couples only the $|\uparrow\rangle$ states to the same Rydberg state $|r\rangle$ (cf. Fig. 2). The first pulse gives all plaquettes with n particles in $|\downarrow\rangle$ a phase ϕ_n, whereas the second pulse gives all plaquettes with $4-n$ particles in the $|\uparrow\rangle$ state a phase ϕ_{4-n}. Due to the Rydberg-Rydberg interaction between atoms in state $|r\rangle$, the phases can be programmed to satisfy $\phi_1 + \phi_3 = \gamma$, and $\phi_0 + \phi_4 = 2\phi_2 = -\gamma$.

We assume that the 2×2 plaquettes can be individually addressed with a Rydberg excitation laser with a time-dependent Rabi frequency $\Omega(t)$, and detuning $\Delta(t)$. The first pulse couples only the $|\downarrow\rangle$ to the Rydberg state, and in this case the relevant Hamiltonian is of the form

$$\begin{aligned}\hat{H}_{2\times2} = &\sum_i \left[-\Delta(t)\,|r_i\rangle\,\langle r_i| + \frac{\Omega(t)}{2}\,|r_i\rangle\,\langle\downarrow_i| + \text{H.c.}\right] \\ &+ \sum_{i<j} V_{ij}|r_i r_j\rangle\langle r_i r_j|,\end{aligned} \tag{4}$$

where the sums run over the indices i, j on the plaquette, and V_{ij} is the van der Waals interaction energy between atoms i and j. Since the desired gate operation is permutation symmetric, it is beneficial to have $V_{ij} = V$. We therefore assume that each plaquette of atoms forms a tetrahedral configuration, which can be realized in a scalable manner by displacing every second lattice diagonal out of a square lattice (see SM [36]). We note however, that this is not a strict requirement (see SM [36]).

For designing our phase gate, we will exploit properties of the many-body eigenspectrum of Eq. (4), obtained by exact diagonalization of $\hat{H}_{2\times2}$, showing the relevant eigenstates in Fig. 2. Since (during the first pulse) we are only coupling the $|\downarrow\rangle$ states, the particles in $|\uparrow\rangle$ remain in a noninteracting ground state, and do not participate in the dynamics. In particular, they can not be excited to the Rydberg state, and the number of relevant eigenstates of Eq. (4) is therefore dependent on the number of particles originally in state $|\downarrow\rangle$ at the start of the pulse, as illustrated in Fig. 2, top row. Dashed lines indicate product eigenstates in the limit $\Omega = 0$, whereas solid, colored, lines are the eigenstates for a specific $\Omega > 0$. If there are initially no particles in $|\downarrow\rangle$ [panel (a)], there is just one eigenstate, i.e. $|\uparrow\uparrow\uparrow\uparrow\rangle$. If there is one particle in the plaquette in state $|\downarrow\rangle$, an additional eigenstate appears, with one particle in $|r\rangle$. For $\Omega = 0$ (dashed line), this state has an energy $-\Delta$. For $\Omega > 0$ this state forms an anticrossing with the original product ground state. Similarly, for $n = 2, 3, 4$ particles in $|\downarrow\rangle$ [panels (c), (d), (e)], more coupled eigenstates with n particles in $|r\rangle$ appear with slopes $-n\Delta$. Moreover, these states have an energy offset at $\Delta = 0$ due to the interactions, equal to $n(n-1)V/2$. It should be noted that the widths of the anticrossings in the spectrum also increase with n.

We now design pulses $\{\Omega(t), \Delta(t)\}$, adiabatically connecting the initial product state of ground state atoms to one of the many-body eigenstates. The initial value of

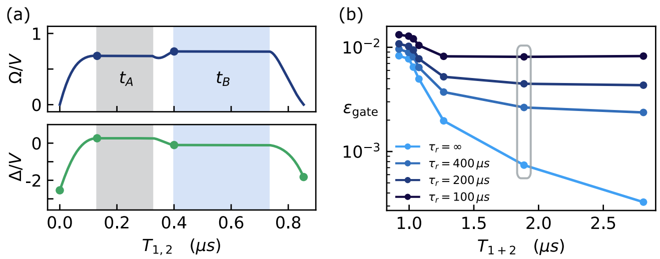

FIG. 3. (a) Two pause pulse example. Laser parameters that are used for pulse optimization are indicated as dots (see main text). (b) Gate error of the parity gate for experimental conditions as: $V = 2\pi \times 40\,\mathrm{MHz}$, $\Omega_{\max} = 2\pi \times 30\,\mathrm{MHz}$, $\Delta_{\mathrm{start,end}}/V \in [-3.0, 0.0]$, $\Delta_{A,B}/V \in [-3.0, 1.0]$, averaged over 10^4 randomly chosen phase-combinations (see SM [36]). Highlighted points correspond to the pulse shown in panel (a), with pause-times $t_{A,B}$ adjusted to $\gamma = \pi/4$, corresponding to the maximally entangling gate operation.

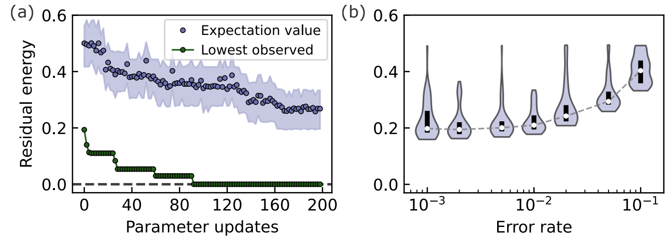

FIG. 4. (a) Example QAOA simulation for 20 qubits. Shown are the lowest observed- and average residual energy after each parameter update. (b) Distribution of average residual energies of 50 independent optimization runs (200 parameter updates) for a single optimization problem with varying error rates of the four-body parity gate. Final energy values were re-estimated via 5000 circuit executions and measurements. The black bars visualize the 25th to 75th percentiles and the white circles denote the median of the distribution.

the detuning at $t = 0$ and $\Omega(0) = 0$ determines to which of the eigenstates we connect when increasing $\Omega > 0$. For example, $\Delta(0) < 0$ connects us to the lowest eigenstate, and $0 < \Delta(0) < V/2$ connects to the first excited state [small arrows in Fig. 2(c)]. For illustrative purposes, we operate on the first excited many-body state. After adiabatically increasing $\Omega > 0$ and subsequently sweeping the detuning back and forth (arrows in Fig. 2), the plaquettes pick up a dynamical phase (the time integral of the particular eigenenergy-trajectory, indicated as shaded areas in Fig. 2), which is dependent on the number n, due to the many-body spectrum depending on n. We can achieve the desired effect that the odd and even plaquettes pick up equal and opposite phases $\pm\gamma$ by repeating the pulse in exactly the same fashion, but this time coupling the $|\uparrow\rangle$ ground states to the Rydberg state (panels (f) - (j) in Fig. 2). By simultaneously illuminating plaquettes that are separated by a line of non-illuminated atoms (see highlighted plaquettes in Fig. 1) to avoid crosstalk between plaquettes, the whole many-body phase gate $e^{-i\gamma \hat{H}_C}$ can be realized in 9 illumination rounds independent of system size.

Two pause protocol– We now discuss how arbitrary plaquette phases γ can be implemented using a two-pause protocol, only requiring onetime optimization and calibration of laser pulse-shapes. Our protocol relies on adiabatic trajectories $(0, \Delta_{\mathrm{start}}) \rightarrow (\Omega_A, \Delta_A) \rightarrow (\Omega_B, \Delta_B) \rightarrow (0, \Delta_{\mathrm{end}})$, where the corresponding laser-pulse is held ("paused") at $(\Omega_{A,B}, \Delta_{A,B})$ for durations $t_{A,B}$ [cf. Fig. 3(a)]. The key observation is that for an arbitrary gate phase γ in Eq. (3), there exists an analytic solution of hold times $t_{A,B}$, realizing the desired phase (see SM [36]). The precise solutions, and hence the total gate duration, depend on the values of $\mathbf{\Omega} = (\Omega_A, \Omega_B)$ and $\mathbf{\Delta} = (\Delta_{\mathrm{start}}, \Delta_A, \Delta_B, \Delta_{\mathrm{end}})$, and the adiabatic path connecting them.

We determine the waypoints $(\mathbf{\Omega}, \mathbf{\Delta})$ of the adiabatic path by numerically optimizing the total gate duration for all values of $\gamma \in [0, 2\pi]$, for the worst case scenario, and given experimental constraints such as achievable interaction strengths V and maximum Rabi frequencies Ω. The paths $\Omega(t), \Delta(t)$, connecting the waypoints $(\mathbf{\Omega}, \mathbf{\Delta})$, are calculated using a novel numerical approach based on quantum adiabatic brachistochrones (QAB) [41–43] (see SM [36], which includes Refs. [44–48]). Once this one-time optimization is done, executing QAOA consists of only varying the hold times $t_{A,B}$, irrespective of the precise problem.

Gate performance– We now assess the performance of our parity gate protocol for a realistic experimental scenario. We assume an interaction strength $V = 2\pi \times 40\mathrm{MHz}$, e.g. achievable for $68S$ states of ^{87}Rb, and particles spaced at 5μm. In the SM [36] we provide a detailed discussion of potential considerations, including three- and four-body effects. We note that for interaction strengths of this magnitude and μs gate operation times, trapping with about $1-2$mK deep traps of the Rydberg states would be required [49, 50], to minimize or prevent excitations of higher motional states in the tweezer traps and their associated fluctuations in interaction strengths, which would adversely affect gate fidelities. The lifetime of the $68S$ states at 300 K is about $150\mu s$ [51].

For parameters in this regime, Fig. 3(b) analyzes the average gate-error $\epsilon_{\mathrm{gate}} = 1 - \overline{\mathcal{F}}$, where $\overline{\mathcal{F}}$ denotes the mean of the average gate fidelity over 10^4 gate realizations, i.e. γ-values. We optimized the laser-parameters in the coherent, i.e. noiseless, regime for various levels of adiabaticity using a 100-steps basin-hopping algorithm [52]. There, the gate error [see light blue line in Fig. 3(b)] solely originates from diabatic errors and thus can be arbitrarily reduced by making the gate more adiabatic, i.e. slower. However, the finite lifetime of Rydberg states restricts the maximal gate-duration and thus limits the achievable gate-performance. Including dissipation (see SM [36], which includes Refs. [53–55]) shows that the best possible gate-performance is a trade-off between diabatic and dissipative error mechanisms [see Fig. 3(b)].

QAOA simulations–We numerically demonstrate the feasibility of our parity-QAOA implementation on small test-scale problems of $K = 20$ qubits (see Fig. 4), arranged in a 4×5 grid, with local fields J_j randomly chosen to be either -1 or 1. This corresponds to a small example optimization problem of a bipartite graph involving 9 logical qubits. Our main objective is to investigate the robustness of our QAOA scheme under varying (depolarizing) noise levels of the four-qubit parity gate (see SM [36], which includes Refs. [56, 57]). We numerically simulated the QAOA circuit Eq. (2) with circuit depth $p = 3$ for various error rates of the four-body gate, while keeping single-qubit error rates constant at 0.05%. Figure 4(a) shows the residual energy $E_{\text{res}} = (\langle E \rangle - E_{\min})/(E_{\max} - E_{\min})$, as function of the number of parameter updates for a sample experiment with a four-qubit error rate of 0.1%. Furthermore, Fig. 4(b) shows that the performance is robust against error rates up to a few percent, which can be achieved with sub-μs Rydberg gate protocols [cf. Fig. 3(b)].

Conclusion and Outlook– While present day Rydberg experiments have seen enormous progress in quantum state control and particle numbers, their focus has been so far predominantly on quantum simulation. Our proposed Rydberg parity gate will enable these experiments to explore solving arbitrary combinatorial optimization problems, providing a new direction towards quantum computing tasks, without requiring substantial hardware changes. We want to emphasize, that our scheme directly relates laser-pulse hold-times to the variational QAOA parameters and thus is a prime example of hardware-algorithm co-design.

The inherent scalability of the parity architecture is naturally complemented by the scalability of the Rydberg platform. We expect intermediate scale Rydberg experiments with up to hundreds of atoms to be able to investigate parity-QAOA in regimes where it cannot be investigated by classical simulations anymore. Going beyond these system sizes, the Rydberg lifetimes will become an issue, and will require either larger interaction strengths for faster gate operations, or modified implementations suited for circular Rydberg states with much longer lifetimes [58–60].

We thank A. M. Kaufman and H. Pichler for helpful discussions. QAOA simulations were performed using qiskit [61]. The work is supported by the European Union program Horizon 2020 under Grants Agreement No. 817482 (PASQuanS), and by the Austrian Science Fund (FWF) through a START grant under Project No. Y1067-N27 and the SFB BeyondC Project No. F7108-N38, the Hauser-Raspe foundation. This material is based upon work supported by the Defense Advanced Research Projects Agency (DARPA) under Contract No. HR001120C0068. Any opinions, findings and conclusions or recommendations expressed in this material are those of the author(s) and do not necessarily reflect the views of DARPA.

[1] F. Arute *et al.*, Quantum supremacy using a programmable superconducting processor, Nature **574**, 505 (2019).

[2] H.-S. Zhong *et al.*, Quantum computational advantage using photons, Science **370**, 1460 (2020).

[3] Y. Wu *et al.*, Strong Quantum Computational Advantage Using a Superconducting Quantum Processor, Phys. Rev. Lett. **127**, 180501 (2021).

[4] J. Preskill, Quantum Computing in the NISQ era and beyond, Quantum **2**, 79 (2018).

[5] I. H. Deutsch, Harnessing the Power of the Second Quantum Revolution, PRX Quantum **1**, 020101 (2020).

[6] H. Bernien, S. Schwartz, A. Keesling, H. Levine, A. Omran, H. Pichler, S. Choi, A. S. Zibrov, M. Endres, M. Greiner, V. Vuletić, and M. D. Lukin, Probing many-body dynamics on a 51-atom quantum simulator, Nature **551**, 579 (2017).

[7] D. Barredo, V. Lienhard, S. de Léséleuc, T. Lahaye, and A. Browaeys, Synthetic three-dimensional atomic structures assembled atom by atom, Nature **561**, 79 (2018).

[8] H. Pichler, S.-T. Wang, L. Zhou, S. Choi, and M. D. Lukin, Quantum Optimization for Maximum Independent Set Using Rydberg Atom Arrays (2018), arXiv:1808.10816 [quant-ph].

[9] H. Levine, A. Keesling, G. Semeghini, A. Omran, T. T. Wang, S. Ebadi, H. Bernien, M. Greiner, V. Vuletić, H. Pichler, and M. D. Lukin, Parallel Implementation of High-Fidelity Multiqubit Gates with Neutral Atoms, Phys. Rev. Lett. **123**, 170503 (2019).

[10] T. M. Graham, M. Kwon, B. Grinkemeyer, Z. Marra, X. Jiang, M. T. Lichtman, Y. Sun, M. Ebert, and M. Saffman, Rydberg-Mediated Entanglement in a Two-Dimensional Neutral Atom Qubit Array, Phys. Rev. Lett. **123**, 230501 (2019).

[11] I. S. Madjarov, J. P. Covey, A. L. Shaw, J. Choi, A. Kale, A. Cooper, H. Pichler, V. Schkolnik, J. R. Williams, and M. Endres, High-fidelity entanglement and detection of alkaline-earth Rydberg atoms, Nature Physics **16**, 857 (2020).

[12] P. Scholl, M. Schuler, H. J. Williams, A. A. Eberharter, D. Barredo, K.-N. Schymik, V. Lienhard, L.-P. Henry, T. C. Lang, T. Lahaye, A. M. Läuchli, and A. Browaeys, Quantum simulation of 2D antiferromagnets with hundreds of Rydberg atoms, Nature **595**, 233 (2021).

[13] S. Ebadi, T. T. Wang, H. Levine, A. Keesling, G. Semeghini, A. Omran, D. Bluvstein, R. Samajdar, H. Pichler, W. W. Ho, S. Choi, S. Sachdev, M. Greiner, V. Vuletić, and M. D. Lukin, Quantum phases of matter on a 256-atom programmable quantum simulator, Nature **595**, 227 (2021).

[14] G. Semeghini *et al.*, Probing topological spin liquids on a programmable quantum simulator, Science **374**, 1242 (2021).

[15] D. Bluvstein, A. Omran, H. Levine, A. Keesling, G. Semeghini, S. Ebadi, T. T. Wang, A. A. Michailidis, N. Maskara, W. W. Ho, S. Choi, M. Serbyn, M. Greiner, V. Vuletić, and M. D. Lukin, Controlling quantum many-body dynamics in driven Rydberg atom arrays, Science

371, 1355 (2021).
[16] E. Farhi, J. Goldstone, and S. Gutmann, A Quantum Approximate Optimization Algorithm (2014), arXiv:1411.4028 [quant-ph].
[17] E. Farhi and A. W. Harrow, Quantum Supremacy through the Quantum Approximate Optimization Algorithm (2016), arXiv:1602.07674 [quant-ph].
[18] S. Lloyd, Quantum approximate optimization is computationally universal (2018), arXiv:1812.11075 [quant-ph].
[19] E. Farhi and A. W. Harrow, Quantum supremacy through the quantum approximate optimization algorithm (2019), arXiv:1602.07674 [quant-ph].
[20] M. E. Morales, J. D. Biamonte, and Z. Zimborás, On the universality of the quantum approximate optimization algorithm, Quantum Information Processing **19**, 1 (2020).
[21] L. Zhou, S.-T. Wang, S. Choi, H. Pichler, and M. D. Lukin, Quantum Approximate Optimization Algorithm: Performance, Mechanism, and Implementation on Near-Term Devices, Phys. Rev. X **10**, 021067 (2020).
[22] J. R. McClean, S. Boixo, V. N. Smelyanskiy, R. Babbush, and H. Neven, Barren plateaus in quantum neural network training landscapes, Nature communications **9**, 1 (2018).
[23] S. Bravyi, A. Kliesch, R. Koenig, and E. Tang, Obstacles to variational quantum optimization from symmetry protection, Phys. Rev. Lett. **125**, 260505 (2020).
[24] V. Akshay, H. Philathong, M. E. S. Morales, and J. D. Biamonte, Reachability deficits in quantum approximate optimization, Phys. Rev. Lett. **124**, 090504 (2020).
[25] V. Akshay, H. Philathong, I. Zacharov, and J. Biamonte, Reachability deficits in quantum approximate optimization of graph problems, Quantum **5**, 532 (2021).
[26] F. G. S. L. Brandao, M. Broughton, E. Farhi, S. Gutmann, and H. Neven, For fixed control parameters the quantum approximate optimization algorithm's objective function value concentrates for typical instances (2018), arXiv:1812.04170 [quant-ph].
[27] E. Farhi, J. Goldstone, S. Gutmann, and L. Zhou, The Quantum Approximate Optimization Algorithm and the Sherrington-Kirkpatrick Model at Infinite Size (2020), arXiv:1910.08187 [quant-ph].
[28] M. Streif and M. Leib, Training the quantum approximate optimization algorithm without access to a quantum processing unit, Quantum Science and Technology **5**, 034008 (2020).
[29] M. M. Wauters, E. Panizon, G. B. Mbeng, and G. E. Santoro, Reinforcement-learning-assisted quantum optimization, Phys. Rev. Research **2**, 033446 (2020).
[30] V. Akshay, D. Rabinovich, E. Campos, and J. Biamonte, Parameter concentrations in quantum approximate optimization, Phys. Rev. A **104**, L010401 (2021).
[31] Y. Song, M. Kim, H. Hwang, W. Lee, and J. Ahn, Quantum simulation of Cayley-tree Ising Hamiltonians with three-dimensional Rydberg atoms, Phys. Rev. Research **3**, 013286 (2021).
[32] W. Lechner, P. Hauke, and P. Zoller, A quantum annealing architecture with all-to-all connectivity from local interactions, Sci. Adv. **1**, e1500838 (2015).
[33] K. Ender, R. ter Hoeven, B. Niehoff, M. Drieb-Schön, and W. Lechner, Parity quantum optimization: Compiler (2021), arXiv:2105.06233 [quant-ph].
[34] A. W. Glaetzle, R. M. W. van Bijnen, P. Zoller, and W. Lechner, A coherent quantum annealer with Rydberg atoms, Nature Communications **8**, 15813 EP (2017).
[35] W. Lechner, Quantum Approximate Optimization With Parallelizable Gates, IEEE Transactions on Quantum Engineering **1**, 1 (2020).
[36] Reference to Supplemental Material.
[37] A. Rocchetto, S. C. Benjamin, and Y. Li, Stabilizers as a design tool for new forms of the Lechner-Hauke-Zoller annealer, Sci. Adv. **2**, e1601246 (2016).
[38] T. Fukuhara, A. Kantian, M. Endres, M. Cheneau, P. Schauß, S. Hild, D. Bellem, U. Schollwöck, T. Giamarchi, C. Gross, I. Bloch, and S. Kuhr, Quantum dynamics of a mobile spin impurity, Nature Physics **9**, 235 (2013).
[39] R. M. W. van Bijnen, C. Ravensbergen, D. J. Bakker, G. J. Dijk, S. J. J. M. F. Kokkelmans, and E. J. D. Vredenbregt, Patterned Rydberg excitation and ionization with a spatial light modulator, New Journal of Physics **17**, 023045 (2015).
[40] H. Labuhn, D. Barredo, S. Ravets, S. de Léséleuc, T. Macrì, T. Lahaye, and A. Browaeys, Tunable two-dimensional arrays of single Rydberg atoms for realizing quantum Ising models, Nature **534**, 667 (2016).
[41] J. Roland and N. J. Cerf, Quantum search by local adiabatic evolution, Phys. Rev. A **65**, 042308 (2002).
[42] S. Jansen, M.-B. Ruskai, and R. Seiler, Bounds for the adiabatic approximation with applications to quantum computation, Journal of Mathematical Physics **48**, 102111 (2007).
[43] A. T. Rezakhani, W.-J. Kuo, A. Hamma, D. A. Lidar, and P. Zanardi, Quantum Adiabatic Brachistochrone, Phys. Rev. Lett. **103**, 080502 (2009).
[44] J. Werschnik and E. K. U. Gross, Quantum optimal control theory, Journal of Physics B: Atomic, Molecular and Optical Physics **40**, R175 (2007).
[45] D. Guéry-Odelin, A. Ruschhaupt, A. Kiely, E. Torrontegui, S. Martínez-Garaot, and J. G. Muga, Shortcuts to adiabaticity: Concepts, methods, and applications, Rev. Mod. Phys. **91**, 045001 (2019).
[46] C. Tsallis and D. A. Stariolo, Generalized simulated annealing, Physica A: Statistical Mechanics and its Applications **233**, 395 (1996).
[47] A. Messiah, *Quantum mechanics*, Vol. 2 (North-Holland, Amsterdam, 1962).
[48] P. Virtanen *et al.*, SciPy 1.0: Fundamental Algorithms for Scientific Computing in Python, Nature Methods **17**, 261 (2020).
[49] R. Mukherjee, J. Millen, R. Nath, M. P. A. Jones, and T. Pohl, Many-body physics with alkaline-earth Rydberg lattices, Journal of Physics B: Atomic, Molecular and Optical Physics **44**, 184010 (2011).
[50] D. Barredo, V. Lienhard, P. Scholl, S. de Léséleuc, T. Boulier, A. Browaeys, and T. Lahaye, Three-Dimensional Trapping of Individual Rydberg Atoms in Ponderomotive Bottle Beam Traps, Phys. Rev. Lett. **124**, 023201 (2020).
[51] I. I. Beterov, I. I. Ryabtsev, D. B. Tretyakov, and V. M. Entin, Quasiclassical calculations of blackbody-radiation-induced depopulation rates and effective lifetimes of Rydberg nS, nP, and nD alkali-metal atoms with $n \leq 80$, Phys. Rev. A **79**, 052504 (2009).
[52] D. J. Wales and J. P. K. Doye, Global Optimization by Basin-Hopping and the Lowest Energy Structures of Lennard-Jones Clusters Containing up to 110 Atoms, *The Journal of Physical Chemistry A*, The Journal of Physical

Chemistry A **101**, 5111 (1997).

[53] M. Saffman, I. I. Beterov, A. Dalal, E. J. Páez, and B. C. Sanders, Symmetric Rydberg controlled-Z gates with adiabatic pulses, Phys. Rev. A **101**, 062309 (2020).

[54] M. A. Nielsen, A simple formula for the average gate fidelity of a quantum dynamical operation, Physics Letters A **303**, 249 (2002).

[55] C. J. Wood, J. D. Biamonte, and D. G. Cory, Tensor networks and graphical calculus for open quantum systems, Quantum Inf. Comput. **15**, 759 (2015).

[56] J. Wurtz and D. Lykov, Fixed-angle conjectures for the quantum approximate optimization algorithm on regular MaxCut graphs, Phys. Rev. A **104**, 052419 (2021).

[57] J. Yao, L. Lin, and M. Bukov, Reinforcement Learning for Many-Body Ground-State Preparation Inspired by Counterdiabatic Driving, Phys. Rev. X **11**, 031070 (2021).

[58] T. L. Nguyen, J. M. Raimond, C. Sayrin, R. Cortiñas, T. Cantat-Moltrecht, F. Assemat, I. Dotsenko, S. Gleyzes, S. Haroche, G. Roux, T. Jolicoeur, and M. Brune, Towards Quantum Simulation with Circular Rydberg Atoms, Phys. Rev. X **8**, 011032 (2018).

[59] F. Meinert, C. Hölzl, M. A. Nebioglu, A. D'Arnese, P. Karl, M. Dressel, and M. Scheffler, Indium tin oxide films meet circular Rydberg atoms: Prospects for novel quantum simulation schemes, Phys. Rev. Research **2**, 023192 (2020).

[60] S. R. Cohen and J. D. Thompson, Quantum Computing with Circular Rydberg Atoms, PRX Quantum **2**, 030322 (2021).

[61] http://qiskit.org.